

吸收光谱法对 Kr 亚稳态浓度测量

褚俊植^{1,3}, 黄珂^{2**}, 栾昆鹏², 胡墅¹, 朱峰², 黄超², 李高鹏², 刘金波¹, 郭敬为¹, 刘栋^{1*}¹中国科学院大连化学物理研究所化学激光重点实验室, 辽宁 大连 116023;²西北核技术研究所激光与物质相互作用国家重点实验室, 陕西 西安 710024;³中国科学院大学, 北京 100049

摘要 近年来光泵浦惰性气体亚稳态激光在高能激光领域逐渐得到人们的关注。搭建了一台高压纳秒脉冲放电产生惰性气体亚稳态粒子的装置, 该装置增益尺寸较长, 便于后续开展激光增益和放大实验。利用窄线宽可调谐连续光源探测了该装置放电生成的 Kr 亚稳态 ($5s[3/2]_2$) 粒子数浓度, 达 $1.3 \times 10^{12} \text{ cm}^{-3}$, 该状态持续时间约为 $3 \mu\text{s}$, 满足后续激光体系运行条件。测量过程中出现了吸收饱和现象, 给粒子数浓度拟合带来了不确定性, 设计的复合拟合方法解决了这一问题。

关键词 光谱学; 激光吸收光谱; 氩亚稳态; 脉冲辉光放电; 稀有气体激光; Voigt 线型

中图分类号 TN248.2

文献标志码 A

doi: 10.3788/CJL202148.0701006

1 引言

近年来, 二极管泵浦碱金属蒸气激光由于好的光束质量、高的量子效率等优点而得到人们的极大关注^[1-4], 但是作为激光增益介质的碱金属蒸气由于活泼的化学性质, 也带来了许多技术难题。如碱金属会造成蒸气池的窗口污染, 同时也会与烷烃类缓冲气体发生化学反应等^[5-6], 这些因素不但导致碱金属蒸气池的寿命缩短, 而且严重影响激光性能。

为解决碱金属蒸气带来的技术难题, 2012 年, Han 等^[7]首次提出一种用亚稳态惰性气体代替碱金属作为激光增益介质的新方案, 并于 2013 年采用 1 kHz 脉冲电源体制备亚稳态 Ar 粒子 (Ar^*), 其粒子数浓度达到 10^{12} cm^{-3} , 随后该团队采用窄线宽的半导体激光器泵浦 Ar^* , 获得了连续脉冲激光^[8]。此后, Rawlins 等^[9]采用频率为 900 MHz 的微波阵列连续放电方式, 利用掺 Ti 蓝宝石可调谐连续激光器对 Ar^* 进行泵浦, 光光效率高达 55%, 这也是目前为止所报道的光光效率的最大值。Han 等^[10-11]

利用纳秒高重频放电技术实现光泵浦 Ar 亚稳态激光器的连续光输出, 输出功率高达 4 W。2019 年, Sanderson 等^[12]首次实现亚稳态 Xe 的激光输出, 由于亚稳态 Xe 较宽的吸收光谱, 在未来有望实现半导体泵浦 Xe 大功率激光输出。在实验迅速发展的同时, 众多实验室针对光泵浦惰性气体激光的增益特性开展了理论模拟工作^[13-14]。

本文对亚稳态 Kr 激光体系进行了初步的探索性研究, 主要工作: 搭建了一台高压纳秒脉冲放电产生惰性气体亚稳态粒子的装置, 并利用窄线宽可调谐连续光源探测了该装置放电生成的 Kr 亚稳态 ($5s[3/2]_2$) 粒子数浓度, 结果表明亚稳态粒子数浓度可达 10^{12} cm^{-3} , 持续时间为 $3 \mu\text{s}$ 。亚稳态粒子数浓度的测定基于比尔吸收定律, 但是由于本文实验装置限制, 出现了吸收饱和现象, 增加了拟合难度。因此设计了一种复合拟合方法, 不仅高精度地拟合出了亚稳态粒子数浓度, 而且给出该状态下粒子能级加宽信息, 为后续激光输出实验提供了设计依据。

收稿日期: 2020-08-25; 修回日期: 2020-10-21; 录用日期: 2020-11-02

基金项目: 激光与物质相互作用国家重点实验室基金 (SKLLIM1913)、国家自然科学基金 (21973093)、中科院化学激光重点实验室创新基金 (KLCL-2019-10)、大连化物所创新研究基金 (DICP I201931)

*E-mail: dongl@dicp.ac.cn; **E-mail: huangke@nint.ac.cn

2 Kr 亚稳态粒子的生成机理和生成装置

2.1 亚稳态 Kr 激光体系

惰性气体基态为满壳层结构,通过激发一个电子到亚稳态,该亚稳态能级结构与碱金属相似。Kr 原子激光体系的能级如图 1 所示,处于基态的粒子通过放电的方式大量富集到第一电子激发态 $5s[3/2]_2$ (记为 Kr^*), 又称之为亚稳态。该能级上的粒子向基态跃迁是禁阻的,其寿命可达数毫秒,因此该能级可以作为激光体系的基态能级。通过窄线宽泵浦光(波长为 811.3 nm)将该亚稳态粒子泵浦到 $5p[5/2]_3$ 能级,在缓冲气体的作用下, $5p[5/2]_3$ 能级上的粒子会迅速弛豫到 $5p[1/2]_1$ 能级,形成粒子数反转并实现 892.8 nm ($5p[1/2]_1 \rightarrow 5s[3/2]_2$) 激光输出。

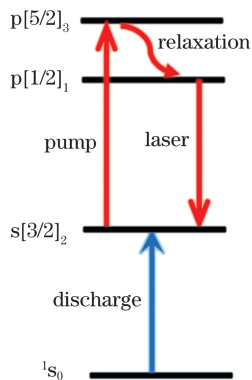


图 1 亚稳态 Kr 三能级激光体系能级示意图

Fig. 1 Schematic of energy levels of three-level laser system for metastable Kr

2.2 亚稳态粒子的生成装置

亚稳态粒子的大量生成可以通过高压等离子放电来实现,高压放电装置将 Kr 原子激发到各电子激发态甚至是电离态,电离态上的粒子经过一段时间回落到亚稳态 $5s[3/2]_2$ 。设计的一套装置结构如图 2 虚线框所示。放电腔体是一个三通腔体,采用高压脉冲直流放电的形式,使用平板电极,通过紫外光预电离的方式实现稳定的辉光放电,放电机理可参见相关工作^[15-16]。输入电压为 15 kV,两平板间距为 15 mm,电极板长度为 12 cm,腔体充入气压为 10.7 kPa 的 Kr 气,其纯度为 99.999%。

3 实验分析涉及的理论

3.1 亚稳态粒子的浓度测定原理

放电生成亚稳态粒子数浓度是评价该装置的重

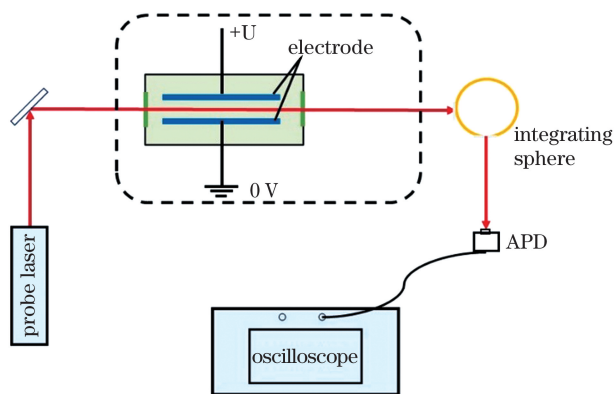


图 2 测量吸收实验装置示意图

Fig. 2 Schematic of the experimental setup for absorption experiment

要指标,这直接影响未来亚稳态激光器的增益特性。采用可调谐连续光源来探测该装置生成的亚稳态粒子数浓度。探测装置如图 2 所示,主要由探测光源和剩余光检测装置两部分组成。探测光源由 760 nm 固体光源泵浦 Cr:LiSAF 晶体获得,输出功率接近 20 mW 的可调谐连续激光,调谐范围为 800~850 nm,输出激光线宽为 70 MHz。探测光从放电装置的两电极板中间穿过,因为探测光的波长覆盖 $5s[3/2]_2 \rightarrow 5p[5/2]_3$ 间的吸收谱线,所以探测光在电极板间传输过程中存在吸收损耗,探测光离开放电装置后进入剩余光测量系统。由于放电装置产生大量的热,探测光光束质量的退化和偏振,剩余探测光先经积分球接受匀化后再传递给 APD 120A 光电探测器,由示波器记录剩余光强度随时间的变化曲线。实验记录了不同中心波长的探测光的剩余光曲线,其中探测中心波长调制间隔为 3~5 pm。另外,为了检验放电电极板间的均匀性,采集过程中不断改变探测光入口位置,但是探测光在放电区的路径长度是相等的,采用上述方法测量了探测光沿不同路径对应的吸收曲线。

探测光通过均匀的待测气体并被吸收的过程可以用比尔定律来描述,比尔定律表达式为

$$I_L = I_0 e^{-\alpha(\nu)NL}, \quad (1)$$

式中: I_0 和 I_L 分别为放电腔体入口和出口处的光强; N 为粒子数浓度; L 为放电区长度; $\alpha(\nu)$ 为中心频率为 ν 的探测光对应的吸收截面。吸收截面^[17]可以表达为

$$\alpha(\nu) = \frac{g_u}{g_l} \frac{A\lambda^2}{8\pi n^2} g(\nu), \quad (2)$$

式中: g_u 和 g_l 分别为吸收对应的上下能级的简并度,其值分别为 7 和 5; λ 为能级吸收的中心波长; n

为折射率; A 为能级吸收的爱因斯坦系数, 其值为 $34.8 \times 10^6 \text{ s}^{-1[18]}$; $g(\nu)$ 为归一化的吸收线型函数, $g(\nu)$ 在全频率空间的积分值为 1。

在探测过程中, 保持放电装置的状态和参数不变, 只改变探测光中心频率, 对放电装置产生的亚稳态粒子进行吸收检测, 并记录了相应的剩余光强度随时间的变化曲线。在此情况下, (1) 式可改写为

$$\alpha(\nu) = \frac{1}{NL} \ln \frac{I_0}{I_L(\nu)}, \quad (3)$$

式中: $I_L(\nu)$ 为中心频率为 ν 的探测光通过放电装置后的剩余光强度。通过扫描中心波长吸收谱线, 可以得 $\ln [I_0/I_L(\nu)]$ 随探测光频率的变化关系曲线, 该曲线与吸收线型函数 $g(\nu)$ 曲线相似, 两者的商为一常数 K , 即

$$\ln \frac{I_0}{I_L(\nu)} = K \cdot g(\nu). \quad (4)$$

常数 K 可以通过非线性最小二乘法拟合获得。 $g(\nu)$ 是归一化线型, 结合 (2)~(4) 式, 可得放电装置中的亚稳态粒子数浓度的表达式为

$$N = \frac{g_1}{g_u} \times \frac{8\pi n^2 K}{A\lambda^2 L}. \quad (5)$$

3.2 Voigt 线型拟合原理及 Kr 吸收谱线线型分析

惰性气体激光器的增益介质为气体介质, 其谱线存在多普勒和碰撞两种加宽机制, 这里对其进行简要描述。碰撞加宽为均匀加宽, 其归一化线型函数^[17]为

$$L(\nu) = \frac{1}{2\pi} \times \frac{\Delta\nu_c}{\nu^2 + (\Delta\nu_c/2)^2}, \quad (6)$$

式中: $\Delta\nu_c$ 为线型的半峰全宽。多普勒加宽为非均匀加宽, 其归一化线型函数^[17]为

$$G(\nu) = \frac{1}{\sigma\sqrt{2\pi}} \times \exp\left(-\frac{\nu^2}{2\sigma^2}\right), \quad (7)$$

式中: σ 为线型的标准差, σ 与多普勒加宽的半峰全宽 $\Delta\nu_D$ 比值为一个常数。综合加宽实质是两种加宽的卷积^[19-20], 即 (4) 式中的线型函数 $g(\nu)$ 表达式为

$$g(\nu) = \int_{-\infty}^{\infty} G(\alpha)L(\nu - \alpha)d\alpha. \quad (8)$$

(8) 式是积分表达式, 直接用来拟合解析式会带来不便和引入误差。解决上述问题的通行方法^[21-22]是将 (8) 式变型为含特殊函数的表达式后再进行拟合操作, (8) 式变型后的表达式为

$$g(\nu) = \frac{\text{Re} [\text{Fad}(z)]}{\sigma\sqrt{2\pi}}, \quad z = \frac{\nu + i(\Delta\nu_c/2)}{\sigma\sqrt{2}}, \quad (9)$$

式中: $\text{Fad}(\cdot)$ 为 Faddeeva 函数, 该函数的具体求解参考文献[23]。

Voigt 线型拟合可以拟合出综合加宽的半峰全宽, 但很难拟合出 $\Delta\nu_c$ 和 $\Delta\nu_D$ 的真实值, 但是可以引入实验中的其他信息来确定 $\Delta\nu_c$ 和 $\Delta\nu_D$ 。高压放电不仅可以产生亚稳态 Kr 粒子, 也会导致气体中的温度升高, 进而影响亚稳态 Kr 粒子的吸收谱线宽度。在垂直于探测光传输方向测量了放电过程气体介质的连续谱线, 通过维恩定理计算^[24]得到放电过程气体介质温度, 该值处于 10000~12000 K。多普勒加宽的半峰全宽的表达式^[17]为

$$\Delta\nu_D = 7.16 \times 10^{-7} \nu_0 \sqrt{T/M}, \quad (10)$$

式中: ν_0 为吸收谱线的中心频率; T 为开尔文温度; M 为 Kr 的原子量。计算得到 $\Delta\nu_D$ 为 3 GHz。实验条件下的 $\Delta\nu_c$ 可参考文献[25]的经验公式, 该公式是拟合 2000~4000 K 的实验值得到的, 通过外推法计算获得本实验条件下的 $\Delta\nu_D$ 为 5.4 GHz。由于该值没有实验支持, 仅能作为参考值, $\Delta\nu_c$ 只能通过 (4) 式和 (9) 式进行拟合获得。

4 分析与讨论

实验装置中的高压放电导致探测光吸收曲线带有很强的噪音, 这将严重影响后续分析。因此对探测信号进行了小波去噪^[26-27]处理, 处理后选取 4 条具有标志性特点的曲线, 如图 3 所示, 结果表明, 剩余光在 15.8 μs 时达到最小值。随着探测光波长向吸收谱线的中心波长移动, 探测光吸收率逐渐增大, 甚至在吸收中心频率 (811.29 nm) 附近出现了吸收饱和现象。

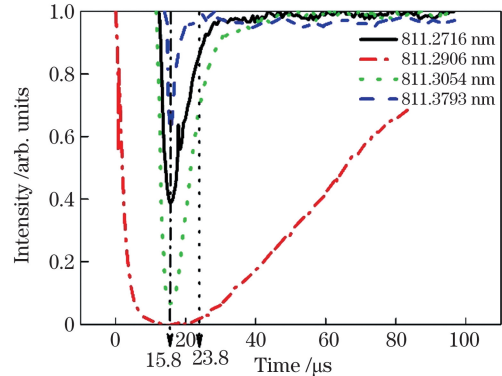


图 3 不同探测波长的剩余探测光强度随时间的变化曲线
Fig. 3 Residual probe light intensity with different wavelengths varying with time

亚稳态粒子数最大浓度值是判断实验装置质量的重要指标。图 3 中的每一条曲线分别对应不同频

率探测光的吸收曲线,各频率探测光的吸收曲线均在 15.8 μs 降到最小值,该值对应(4)式中的 $I_L(\nu)$,代入(4)式进行拟合操作,拟合效果如图 4 所示。由于图 3 显示了在中心波长附近出现的探测光吸收饱和现象,为了提高拟合精度,在拟合过程中去除了吸收率大于 95% 的数据点。虽然如此,拟合结果未能体现真实情况。例如拟合得到的 $\Delta\nu_C$ 为 22 GHz,拟合结果与文献[24]中实验得到的参考值有差距。造成这一结果的原因是中心波长对应的数据缺失和拟合方程中未知变量太多。通过改变气压和放电区间的长度,可避免图 3 中的饱和现象。但本装置是精心优化的产物,改变气压后会给放电装置带来不稳定性;同样减小放电区的长度也不可取,一方面这会降低未来激光器的增益长度,另一方面需要对放电装置进行较大的改动。另外,吸收饱和现象是放电装置质量高的表现,这意味着亚稳态粒子数浓度达到较高的值。

因为多普勒半峰全宽 $\Delta\nu_D$ 已通过(10)式得到,采用(4)式拟合不同频率下的吸收强度,将获得 K

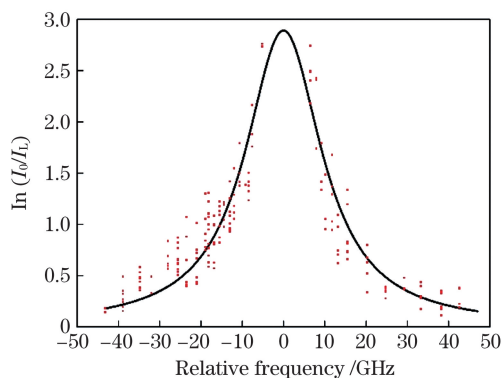


图 4 吸收谱线的测量数据和传统方法拟合的曲线(实线)
Fig. 4 Measured data of absorption spectrum line and fitting profile (solidline) by traditional fitting method

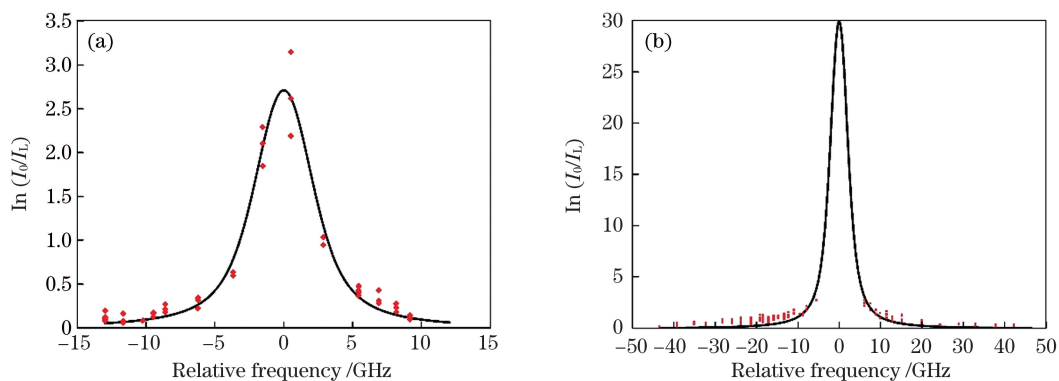


图 5 不同时刻吸收谱线的测量数据和拟合曲线。(a) 23.8 μs ; (b) 15.8 μs
Fig. 5 Measured data and fitting profile of absorption spectrum line at different time. (a) 23.8 μs ; (b) 15.8 μs

和碰撞加宽半峰全宽 $\Delta\nu_C$ 两个值。仔细观察图 4 可以发现,饱和吸收现象导致中心频率附近数据缺失,缺失的频率高达 12 GHz,这是 $\Delta\nu_C$ 拟合误差过大的直接原因。为此设计一种复合拟合法解决上述问题,该方法先选用探测光不饱和时刻的实验数据拟合 $\Delta\nu_C$,该时刻也可以得到一个 K 值,代入(5)式后得到该不饱和时刻对应的浓度值(该值要小于最大浓度);将前面拟合得到的 $\Delta\nu_C$ 代入(9)式中,再结合(4)式拟合图 4 的实验数据,得到一个新 K 值,根据(5)式即可计算得到亚稳态粒子数最大浓度。

图 3 中 23.8 μs 对应的剩余光均未达到饱和,可用来拟合 $\Delta\nu_C$,拟合结果如图 5(a)所示,拟合得到的 $\Delta\nu_C$ 为 3.29 GHz,该时刻对应的粒子数浓度为 $1.45 \times 10^{11} \text{ cm}^{-3}$,拟合得到的 $\Delta\nu_C$ 与参考文献[25]的经验公式计算的参考值较为接近。将 $\Delta\nu_C$ 的拟合结果代入(8)式中,即可得到线型函数 $g(\nu)$,再结合(4)式即可拟合亚稳态粒子数最大浓度,拟合结果如图 5(b)所示,计算得到亚稳态粒子数最大浓度为 $1.38 \times 10^{12} \text{ cm}^{-3}$ 。此外,拟合过程中采用的实验数据来源于电极板间相同长度的不同传输路径,拟合结果表明,它们均匀分布在拟合曲线附近,这证明了本实验放电产生的亚稳态粒子数浓度是较为均匀的。

计算表明,在放电电压为 15 kV, Kr 压力为 10.7 kPa 条件下,粒子能级表现为典型的混合加宽,综合半峰全宽约为 5 GHz,其中多普勒半峰全宽和碰撞加宽半峰全宽均为 3 GHz。由加宽机制可知,该条件下其他能级也具有相同的加宽效果。上述数据可以引入速率方程中,为下一步的激光体系设计提供依据。

根据拟合得到的吸收系数曲线,可以计算出放电过程中亚稳态粒子数浓度随时间的变化关系,结果如图 6 所示。结果表明,放电开关打开,亚稳态粒

子数浓度开始上升,从 $9 \mu\text{s}$ 开始迅速上升,在 $15.8 \mu\text{s}$ 处达到最大,然后由于碰撞弛豫、交叉弛豫、辐射跃迁等效应,粒子数减少。其中 $23.8 \mu\text{s}$ 对应的粒子数浓度与图 5(a)拟合的值一致,这表明本复合拟合方法是有效的。图 6 中,将 $9 \mu\text{s}$ 之前的数据舍去的原因是放电的干扰导致无法提取该段时间的变化数据。图 6 显示亚稳态粒子数浓度高于 10^{12}cm^{-3} 的时间约为 $3 \mu\text{s}$,理论上可以满足后续激光运行的要求。

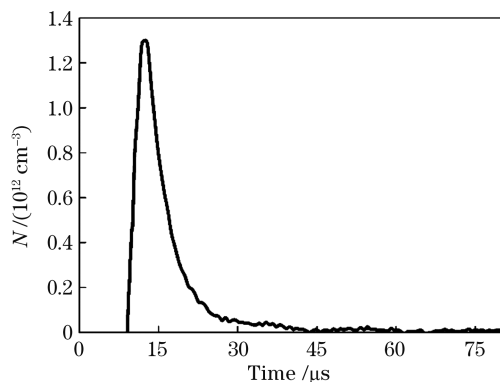


图 6 粒子数浓度随时间的变化

Fig. 6 Variation of particle number concentration with time

5 结 论

搭建了一台可用于产生高浓度惰性气体亚稳态的纳秒高压脉冲放电装置,并采用可调谐固体激光吸收光谱方法对亚稳态 Kr 粒子产生时间和浓度进行了表征。结果表明该装置在 15 kV 的放电电压下,生成的 Kr 亚稳态粒子数浓度可达 $1.3 \times 10^{12} \text{cm}^{-3}$,粒子数浓度高于 10^{12}cm^{-3} 的时间为 $3 \mu\text{s}$,完全满足后续光泵浦亚稳态惰性气体激光对放电激励源的要求。在后续实验中,将对电极形状和放电方式进行相关探索研究,在保证稳定的辉光放电的条件下,进一步提高 Kr 亚稳态粒子数浓度。还设计了一种复合拟合方法,用于解决饱和和吸收条件下粒子数浓度的计算问题,该方法具有普适性。该方法不仅提高了粒子数浓度的计算精度,还得到了能级加宽信息。该装置在放电条件下的能级加宽为混合加宽,半峰全宽为 5 GHz ,这可以为 Kr 亚稳态激光系统提供设计依据。

参 考 文 献

- [1] Beach R J, Krupke W F, Keith Kanz V, et al. End-pumped continuous-wave alkali vapor lasers: experiment, model, and power scaling[J]. Journal of the Optical Society of America B, 2004, 21(12): 2151-2163.
- [2] Li Y, Hua W, Li L, et al. Experimental research of a chain of diode pumped rubidium amplifiers [J]. Optics Express, 2015, 23(20): 25906-25911.
- [3] Endo M. Pulsed output generation in a diode-pumped cesium vapor laser using the cavity dumping technique[J]. Optics Letters, 2019, 44(6): 1312-1314.
- [4] Xu C, Tan R Q, Li Z Y, et al. 2.8 W linearly polarized output of rubidium vapor laser with diode pumping[J]. Chinese Journal of Lasers, 2013, 40(1): 0102009.
徐程, 谭荣清, 李志永, 等. 半导体抽运铷蒸气输出 2.8 W 线偏振铷激光[J]. 中国激光, 2013, 40(1): 0102009.
- [5] Tam A, Moe G, Happer W. Particle formation by resonant laser light in alkali-metal vapor[J]. Physical Review Letters, 1975, 35(24): 1630-1633.
- [6] Tanaka T, Mitsui T, Sugiyama K, et al. Shapes of laser-produced CsH particles [J]. Physical Review Letters, 1989, 63(13): 1390-1392.
- [7] Han J D, Heaven M C. Gain and lasing of optically pumped metastable rare gas atoms [J]. Proceedings of SPIE, 2012, 8547: 85470Z.
- [8] Han J D, Glebov L, Venus G, et al. Demonstration of a diode-pumped metastable Ar laser [J]. Optics Letters, 2013, 38(24): 5458-5461.
- [9] Rawlins W T, Galbally-Kinney K L, Davis S J, et al. Optically pumped microplasma rare gas laser [J]. Optics Express, 2015, 23(4): 4804-4813.
- [10] Han J, Heaven M C, Moran P J, et al. Demonstration of a CW diode-pumped Ar metastable laser operating at 4 W [J]. Optics Letters, 2017, 42(22): 4627-4630.
- [11] Yu G Q, Yang Z N, Lu Q S. Research development of diode pumped metastable rare gas laser [J]. Laser & Optoelectronics Progress, 2015, 52(1): 010001.
余光其, 杨子宁, 陆启生. 半导体激光抽运亚稳态惰性气体激光器研究进展 [J]. 激光与光电子学进展, 2015, 52(1): 010001.
- [12] Sanderson C R, Ballmann C W, Han J D, et al. Demonstration of a quasi-CW diode-pumped metastable xenon laser [J]. Optics Express, 2019, 27(24): 36011-36021.
- [13] Yang Z, Yu G, Wang H, et al. Modeling of diode pumped metastable rare gas lasers [J]. Optics Express, 2015, 23(11): 13823-13832.
- [14] Sun P F, Zuo D L, Mikheyev P A, et al. Time-dependent simulations of a CW pumped, pulsed DC discharge Ar metastable laser system [J]. Optics

- Express, 2019, 27(16): 22289-22301.
- [15] Huang C, Huang K, Yi A P, et al. 200 W mid-infrared HF chemical laser with repetition rate [J]. Chinese Journal of Lasers, 2019, 46(8): 0801005. 黄超, 黄珂, 易爱平, 等. 200 W 重复频率中红外氟化氢化学激光器 [J]. 中国激光, 2019, 46(8): 0801005.
- [16] Huang C, Huang K, Yi A P, et al. A mid-infrared pulsed HF chemical laser with 100 Hz repetition rate [J]. Chinese Journal of Lasers, 2019, 46(2): 0201002. 黄超, 黄珂, 易爱平, 等. 100 Hz 重复频率脉冲中红外 HF 化学激光器 [J]. 中国激光, 2019, 46(2): 0201002.
- [17] Zhou B K, Gao Y Z, Chen Z R, et al. Principles of lasers [M]. 4th ed. Beijing: National Defense Industry Press, 2000. 周炳琨, 高以智, 陈侗嵘, 等. 激光原理 [M]. 4 版. 北京: 国防工业出版社, 2000.
- [18] Chang R S F, Horiguchi H, Setser D W. Radiative lifetimes and two-body collisional deactivation rate constants in argon for Kr(4p 55p) and Kr(4p 55p') states [J]. The Journal of Chemical Physics, 1980, 73(2): 778-790.
- [19] Armstrong B H. Spectrum line profiles: the Voigt function [J]. Journal of Quantitative Spectroscopy and Radiative Transfer, 1967, 7(1): 61-88.
- [20] Roston G D, Obaid F S. Exact analytical formula for Voigt spectral line profile [J]. Journal of Quantitative Spectroscopy and Radiative Transfer, 2005, 94(2): 255-263.
- [21] Abrarov S M, Quine B M. Efficient algorithmic implementation of the Voigt/complex error function based on exponential series approximation [J]. Applied Mathematics and Computation, 2011, 218(5): 1894-1902.
- [22] Gautschi W. Efficient computation of the complex error function [J]. SIAM Journal on Numerical Analysis, 1970, 7(1): 187-198.
- [23] Zaghloul M R, Ali A N. Algorithm 916: computing the Faddeyeva and Voigt functions [J]. ACM Transactions on Mathematical Software, 2012, 38(2): 15.
- [24] Koechner W. Thermo-optic effects and heat removal [M]//Solid-state laser engineering. Springer series in optical sciences. Heidelberg: Springer, 1999, 1: 406-468.
- [25] Manoharan R, Boyson T K, O'byrne S. Time-resolved temperature and number density measurements in a repetitively pulsed nanosecond-duration discharge [J]. Physics of Plasmas, 2016, 23(12): 123527.
- [26] Donoho D L. De-noising by soft-thresholding [J]. IEEE Transactions on Information Theory, 1995, 41(3): 613-627.
- [27] Jian R Y. Functional analysis for applied mathematics [M]. Beijing: Science Press, 2013. 蹇人宜. 应用数学中的泛函分析 [M]. 北京: 科学出版社, 2013.

Concentration Measuring of Metastable Kr via Absorption Spectroscopy

Chu Junzhi^{1,3}, Huang Ke^{2**}, Luan Kunpeng², Hu Shu¹, Zhu Feng², Huang Chao²,
Li Gaopeng², Liu Jinbo¹, Guo Jingwei¹, Liu Dong^{1*}

¹Key Laboratory of Chemical Lasers, Dalian Institute of Chemical Physics, Chinese Academy of Sciences, Dalian, Liaoning 116023, China;

²State Key Laboratory of Laser Interaction with Matter, Northwest Institute of Nuclear Technology, Xi'an, Shaanxi 710024, China;

³University of Chinese Academy of Sciences, Beijing 100049, China

Abstract

Objective Diode-pumped alkali-vapor lasers (DPALs) represent a research hotspot in the field of high-power lasers owing to their advantageous properties, such as high efficiency, excellent beam quality, and scalability. However, DPALs are also affected by several issues: (1) alkali-metals are very active and react easily with coating materials of windows, sealant materials, etc., especially at high temperature; therefore, it is very challenging to prepare the sample cell; (2) alkali-metals also react with relaxing gas (methane or ethane) and produce carbon that contaminates windows, thus seriously reducing the windows lifetime of the sample cell. As a consequence, researchers are putting enormous efforts into the exploration of substitutes for alkali-metals. Among these, metastable rare gases are considered to be the most promising candidates. Metastable rare gases have an electronic structure similar to that of

alkali-metals. Therefore, optically-pumped metastable rare-gas lasers (OPRGLs) are expected to have similar properties to DPALs, without any of the disadvantages mentioned above. However, metastable rare gases do not readily exist; they are normally prepared through high-voltage discharge. The density, homogeneity, and stability of metastable rare gases are key factors for OPRGLs.

Methods The discharge system was composed of a simple circuit with a ~ 100 ns pulsed high-voltage power supply and a pair of parallel plate Cu electrodes (Fig. 2). The flat electrode discharge technique was used to produce a metastable state ($5s[3/2]_2$) for Kr (here denoted as Kr^*). The discharge voltage is 15 kV, the distance between electrodes is 1.5 cm, and the electrodes dimensions are 120 mm \times 10 mm. In order to improve the homogeneity and stability of the discharge, a UV light pre-ionization technique was applied. A stainless-steel structure with three windows was used to contain the ultrahigh purity Kr (99.999%). The front and back windows were made of CaF_2 to ensure that the infrared laser could pass through the cell, whereas the side window was made of polymethyl methacrylate. A tunable continuous infrared laser, based on the Cr : LiSAF crystal, was used as the probe laser, offering a tunability from 800 nm to 850 nm with a linewidth of 70 MHz. The output power is above 20 mW at 811 nm, with a pump power of 450 mW. Therefore, the absorption profile could be recorded through scanning the laser frequency with a step of 3–5 pm. After the probe laser passed through the cell, the residual light was collected using an integrating sphere, then detected via an avalanche photodiode (APD 120A). An oscilloscope was used to visualize the absorption curve. In order to evaluate the Kr^* density uniformity, the absorption curves along different paths were recorded separately. Moreover, an Ocean optics HR4000 spectrometer was used to measure the optical emission spectra of the high-voltage DC discharge plasma along the back window.

By means of the Beer theorem, the Kr^* density could be calculated from the residual rate, which is defined as the ratio of the residual probe laser power I_L to its initial value I_0 . The value of $\ln[I_0/I_L(v)]$ is proportional to the absorption profile $g(v)$. $g(v)$ represents the convolution function of the Doppler broadening profile with the pressure broadening profile. The Doppler broadening profile was obtained by analyzing the optical emission spectra, whereas the pressure broadening profile was derived from the fitting process.

Results and Discussions The absorption curve shape (Fig. 3) could be altered upon tuning the frequency of the probe laser. The shape of the absorption curves indicates that the Kr^* density is firstly increased and then decreased. The maximum Kr^* density occurs 15.8 μs after triggering the discharge. It is noticed that the absorptivity saturates as the frequency of the probe laser approaches the resonant frequency of the transition $5s[3/2]_2 \rightarrow 5p[5/2]_3$, which could result in a fitting error. The saturation of all curves disappears 23.8 μs after triggering the discharge. Hence, $g(v)$ could be obtained by fitting the $\ln[I_0/I_L(v)]$ curve starting from 23.8 μs , whereas the maximum Kr^* density was calculated using the experimental data at 15.8 μs (Fig. 5). This new fitting technology is here referred to as complex fitting method. Compared with the results obtained from the traditional fitting method (Fig. 4), the proposed complex fitting method has clear advantages.

The results show that under a discharge voltage of 15 kV, the Kr^* density can reach a magnitude of $1.3 \times 10^{12} \text{ cm}^{-3}$ and last for 3 μs (Fig. 6). The results also indicate that the full width at half maximum of the Kr energy profile is 5 GHz, being equally affected by the Doppler and pressure broadening.

Conclusions In this work, a nanosecond high-voltage pulsed power device was fabricated to generate metastable-state rare gases with high density. The time-resolved density of metastable Kr^* was characterized via tunable continuous laser absorption spectroscopy. The results show that under a discharge voltage of 15 kV, Kr^* can reach a magnitude of $1.3 \times 10^{12} \text{ cm}^{-3}$ and last for 3 μs . These results fully meet the requirements for optically-pumped metastable rare gas lasers. In future experiments, the electrodes shape and discharge mode will be explored to further improve the density of metastable Kr.

In addition, it was shown that a complex fitting method can be used to solve the fitting error caused by the saturated absorption. This method can not only improve the calculation accuracy of metastable Kr, but also provides information on the broadening, which can be used in the rate equations for the Kr metastable laser system.

Key words spectroscopy; laser absorption spectrum; metastable Krypton; pulsed glow discharge; rare gas laser; Voigt line profile

OCIS codes 300.1030; 140.1340; 350.5400; 140.3480